HHS Public Access

Author manuscript

Osteoarthritis Cartilage. Author manuscript; available in PMC 2018 April 01.

Published in final edited form as:

Osteoarthritis Cartilage. 2017 April ; 25(4): 513–520. doi:10.1016/j.joca.2016.09.015.

Cluster Analysis of Quantitative MRI T_2 and $T_{1\rho}$ Relaxation Times of Cartilage Identifies Differences between Healthy and ACL-injured Individuals at 3T

Uchechukwuka D. Monu[1,2], **Caroline D. Jordan**[3], **Bonnie L. Samuelson**[4], **Brian A. Hargreaves**[1,2,5], **Garry E. Gold**[1,5,6], and **Emily J. McWalter**[7]

[1]Department of Radiology, Stanford University, Stanford, California, USA

[2]Department of Electrical Engineering, Stanford University, Stanford, California, USA

[3]Department of Radiology and Biomedical Imaging, University of California San Francisco, California, USA

[4]Department of Human Biology, Stanford University, Stanford, California, USA

[5]Department of Bioengineering, Stanford University, Stanford, California, USA

[6]Department of Orthopaedic Surgery, Stanford University, Stanford, California, USA

[7]Department of Mechanical Engineering, University of Saskatchewan, Saskatoon, SK, Canada

Abstract

PURPOSE—To identify focal lesions of elevated MRI T_2 and $T_{1\rho}$ relaxation times in articular cartilage of an ACL-injured group using a novel cluster analysis technique.

MATERIALS AND METHODS—Eighteen ACL-injured patients underwent 3T MRI T_2 and $T_{1\rho}$ relaxometry at baseline, six months and one year and six healthy volunteers at baseline, one day and one year. Clusters of contiguous pixels above or below T_2 and $T_{1\rho}$ intensity and area thresholds were identified on a projection map of the 3D femoral cartilage surface. The total area of femoral cartilage plate covered by clusters (%CA) was split into areas above (%CA+) and below (%CA−) the thresholds and the differences in %CA(+ or −) over time in the ACL-injured group were determined using the Wilcoxon signed rank test.

Corresponding Author: Emily J. McWalter, emily.mcwalter@usask.ca.

Author Contributions

The authors contributed to this manuscript in the following ways: Conception and design (UDM, BAH, GEG, EJM); Analysis and interpretation of data (UDM, CDJ, BS, BAH, GEG, EJM); Drafting of the article (UDM, EJM); obtaining of funding (BAH, GEG, EJM); Collection and assembly of data (UDM, CDJ). All authors critically revised the manuscript and gave final approval of the article. UDM, BAH, GEG and EJM take responsibility for the integrity of the manuscript as a whole (emily.mcwalter@usask.ca)

Conflict of Interest

Uchechukwuka D. Monu has no conflicting interests. Caroline D. Jordan has no conflicting interests. Bonnie L. Samuelson has no conflicting interests. Brian A. Hargreaves receives research or institutional support from GE Healthcare and NIH, and receives patent royalties from GE Healthcare, Siemens and Philips. Garry E. Gold receives research or institutional support from GE Healthcare, the NIH, and provides consulting services to Boston Scientific. Emily J. McWalter has no conflicting interests.

RESULTS—%CA+ was greater in the ACL-injured patients than the healthy volunteers at six months and one year with average %CA+ of 5.2 ± 4.0% (p=0.0054) and 6.6 ± 3.7% (p=0.0041) for T_2 and 6.2 ± 7.1% (p = 0.063) and 8.2 ± 6.9% (p = 0.042) for $T_{1\rho}$, respectively. %CA− at six months and one year was 3.0 ± 1.8% (p > 0.1) and 5.9 ± 5.0% (p > 0.1) for T_2 and 4.4 ± 4.9% (p > 0.1) and 4.5 ± 4.6% (p > 0.1) for $T_{1\rho}$, respectively.

CONCLUSION—With the proposed cluster analysis technique, we have quantified cartilage lesion coverage and demonstrated that the ACL-injured group had greater areas of elevated T_2 and $T_{1\rho}$ relaxation times as compared to healthy volunteers.

Keywords

quantitative MRI; cartilage; knee; ACL-injury; projection maps; cluster analysis

INTRODUCTION

Anterior cruciate ligament (ACL) ruptures have an annual incidence of 100,000 to 200,000 in the U.S. in individuals between 15–45 years old and have been shown to increase the risk of osteoarthritis (OA)[1,2]. Radiographic OA develops in as many as 50% of ACL-injured knees 10 to 20 years after reconstructive surgery and can only be detected once gross morphological abnormalities have occurred[3–6]. Ideally we would detect OA earlier in the disease process when treatments will likely be more effective. One early characteristic of OA is the depletion and disorganization of the articular cartilage extracellular matrix macromolecules, therefore, imaging techniques have been proposed and developed to detect these changes[7–11]. Changes in quantitative MRI parameters have been shown at six months and one-year post ACL injury[21], making this population important for developing quantitative measures sensitive to these pre-radiographic OA matrix changes.

Advanced MRI techniques offer quantitative assessment of macromolecular changes to the cartilage matrix[7–11]. T_2 and $T_{1\rho}$ relaxation time mapping have demonstrated some ability to track cartilage quality and have been used to study OA[9–13]. T_2 measures the transverse relaxation time and is used to assess the water and collagen content in the cartilage[14,15,18,19] while $T_{1\rho}$, or relaxation in the rotating frame, probes the slow-motion interaction between the motion-restricted water molecules and large macromolecules and is used to assess glycosaminoglycan (GAG) content[9,12,13,17]. Both relaxation parameters have been shown to increase in the ACL-injured population, 1–2 years after reconstructive surgery[20–22].

Previous studies have shown great potential for using quantitative imaging measures to track cartilage health but technical challenges still limit their widespread adoption. Existing segmentation techniques are time-consuming and often prevent use of all of the data. As a result, most studies, especially for 2D imaging, examine only a single slice from the lateral and medial compartments of the knee, often neglecting the trochlear region[23,24]. The choice of slice and definition of sub-regions within each slice varies across investigations, making it hard to compare data across time points or between studies. Averaging within regions or entire segmented slices is another common practice that leads to loss of spatial localization. Magic angle effects[25] cause increased T_2 in the posterior condyles and trochlear region and can erroneously increase the mean of a region if not considered. If areas of increased T_2

relaxation time due to magic angle effects are included in one groups ROI and not another, reported means cannot be compared. Analysis methods that include the whole 3D dataset and take into consideration magic angle effects will allow for identification of focal defects and better comparisons over time and across populations.

Few studies implement advanced processing techniques that look at the heterogeneity of the cartilage quantitative data, full 3D analysis as well as registration for within population and across time-point comparisons. Texture, laminar and Z-score analyses have been used to examine the spatial distribution and heterogeneously quantitative data within the cartilage, showing that the natural heterogeneity of quantitative T_2 and $T_{1\rho}$ values in healthy cartilage, typically increases with OA[26,27,28–32]. These processing techniques have shown promise but to date few investigations look at the full cartilage plate, therefore missing important regions of degeneration, such as the trochlea[30,33]. One challenge to carrying out 3D comparisons is the registration of data between time-points and individuals. One group has proposed a voxel-based relaxometry technique[33] that addresses this issue. This approach was shown to be more sensitive to local patterns in $T_{1\rho}$ relaxation time than traditional ROI-based approaches. Another potential approach, which has been used to study variations in 3D cartilage thickness[34,35], is to use projection maps; these maps could also be used for registration between time-points and for isolating heterogeneity and focal defects. Capturing as much information about pathological changes and improving the detection of these changes is very important for identifying early cartilage degeneration and monitoring therapy.

Focal defects in cartilage are an important pathological change in OA that has received relatively little attention in the quantitative cartilage MRI literature; most work to date has reported mean changes or general heterogeneity. This is important because we know that later in the OA disease process both general cartilage thinning and focal defects are observed[36]. The aim of this work was therefore to develop a new cluster analysis method that identifies focal cartilage lesions and evaluate it as a method to identify differences in 3D T_2 and $T_{1\rho}$ relaxation time mapping data between ACL-injured and healthy individuals.

METHODS

Study Population

All scans were performed in the sagittal plane using two MR750 3T scanners (GE Healthcare, Waukesha, WI) and a volume-transmit, 8 channel-receive knee coil (Invivo Inv., Gainesville, FL). Eighteen ACL-injured patients were scanned at baseline (8–87 days post-surgery), six months post baseline and one-year post baseline[37]. Six healthy volunteers were scanned at baseline, one-day post baseline, and one-year post baseline to determine the reproducibility of the technique and to set the thresholds used for comparing groups. A radiologist with seventeen years of experience (GEG) excluded any healthy volunteer with cartilage defects. Informed consent was obtained and the study was conducted in accordance with the guidelines of the institutional review board.

Imaging Protocol and Quantitative Mapping

$T_{1\rho}$ relaxation times were estimated using a $T_{1\rho}$ magnetization-prepared pseudo-steady-state 3D fast spin echo (FSE) sequence (CubeQuant)[38]. Acquisition parameters: 500 Hz spin-lock pulse frequency, repetition time (TR) = 1228 ms, 90° flip angle, partial *k*-space acquisition using 0.5 averages, a resolution of 0.5 mm × 0.625 mm × 3 mm, 62.5kHz bandwidth, four spin-lock time (TSL) durations of 1 ms, 10 ms, 30 ms, and 60 ms, and a total scan time of 5:49 min. $T_{1\rho}$ relaxation time mapping was carried out by doing a pixel-wise mono-exponential fit to the series of varying TSL images using the equation S(TSL) ~ exp(−TSL/T1ρ) within packaged freeware (OsiriX, Pixmeo Sarl, Bern, Switzerland)[39].

T_2 relaxation times were estimated using a modified, quantitative 3D double-echo in steady-state sequence (DESS) technique[40]. 3D DESS is an established T_2 mapping sequence used and validated in numerous studies[24,40,41,42]. The sequence acquired an echo on either side of an unbalanced spoiler gradient. The first echo has T_1/T_2 contrast (S^+) and the second (S^-) has T_2 and diffusion contrast. The sequence was run twice in succession, first with a small diffusion spoiler gradient area (34.66 ms*mT/m on all three axes) and a large flip angle (35°) (DESS Low/S_1), and second with a large diffusion spoiler gradient area (138.4 ms*mT/m on all three axes) and small flip angle (18°) (DESS Hi/S_2). This results in four images per subject. Specific parameters include: echo times (TE1) of 9 ms (S^+) and TE2 of 43 ms (S^-) (TE2 is the time between the RF pulse from the prior repetition and the echo signal), TR = 26 ms, 1 average, a resolution of 0.625 mm × 0.62 mm × 3 mm, a bandwidth of 32.5kHz and a total scan time of 9:40 min (for both scans). We determined the T_2 relaxation time in a voxel-wise manner using three calculated signal ratios (S_1^-/S_1^+, S_2^-/S_2^+, and S_1^+/S_2^+) and a dictionary created based on the signal model proposed by Wu and Buxton[42]. The dictionary was created once for specified imaging parameters, a range of possible T_1 and T_2 relaxation times and apparent diffusion coefficients (processing time: < 1min). It was then searched for the T_2 relaxation time that minimizes the sum of squared error between the three signal ratios of the measured and modeled values. This analysis was carried out using a custom plugin (OsiriX).

MRI Post-processing

Registration—Many of the sagittal scans acquired had some degree of femoral internal or external rotation, which creates difficulties in registration between time points. Therefore, the 3D image data was reformatted to create registered, anatomically based sagittal images. To accomplish this, a line was drawn through the most posterior points of the medial and lateral femoral condyles. The plane perpendicular to this line was considered the anatomically based sagittal plane. The images were reformatted in OsiriX into this new plane using cubic-spline interpolation (Fig. I-ii).

A custom software package (Matlab, the Mathworks, Natwick, MA) was developed to carry out the modules below:

Segmentation—Slice-by-slice manual segmentation was performed on the $T_{1\rho}$-weighted images with spin-lock time (TSL = 10ms) and on the mean of the magnitude DESS Low images (segmentation time: ~90min/knee). These images provided the best anatomic

contrast for segmentation. Binary masks created from the segmented data were superimposed onto their respective parameter maps for the extraction of the full volume quantitative T_2 and $T_{1\rho}$ relaxation times (Fig. I-iB). Some ACL-injured patient data had metal artifacts due to surgical hardware; in such cases, special care was taken during segmentation to ensure that the distance to the artifact was sufficient and no signal void or pileup was captured (Fig. I-iii).

Projection Map—Projection maps were created for visualization and subsequent cluster analysis. First, the bone-cartilage interface was extracted from each segmented slice and collapsed into a single sagittal plane. A circle was fit to the data using a least-squares approach and the center and radius of this circle were used to create a cylinder that was fit through the femoral condyles (Fig. I-iC). In the original segmented data, the most anterior proximal point was identified in each slice and then rays were drawn at 1° increments from this point to 245°, thereby creating 245 angular bins (Fig. I-iC). This range encompasses all the cartilage across our two groups. Pixel data from cartilage that fell within the bin were averaged. In the case were pixels fell within multiple bins, an area-based weighted-average was used. Projection maps were created by plotting angular bin versus slice number (Fig. I-iD). To obtain isotropic projection maps, interpolation in the slice direction using a 1×10 interpolation factor was performed. A 1×5 low pass, blurring filter was then used to mitigate the effect of noise in the angular bin direction.

Difference Maps—Difference maps were created by subtracting projection maps at different time points. Difference maps decreased magic angle effects still present after the registration step at a band of about ±10° degrees around a ±54° angle from the static magnetic field (46° and 144° in the projection maps). Because there were slight differences in the segmentation of the cartilage edges, any pixel without a corresponding pixel at another time point were removed by erosion using a 7 pixel wide disk. Metal artifacts were manually excluded to reduce through-slice signal pile-up or void artifacts.

Cluster Analysis—Cluster analysis was used to identify focal lesions in the cartilage plates of the ACL-injured group. We classified clusters as either increased or decreased by setting two thresholds – intensity and size. For both T_2 and $T_{1\rho}$ relaxation times, thresholds for increased and decreased clusters were set at $+2\sigma$, where σ is the mean standard deviation of the healthy groups' difference map (Fig. II-B). A cluster was defined as a contiguous set of pixels above or below these thresholds, separated by a maximum of one pixel, corner or edge wise. A histogram of cluster areas within the healthy subjects for both T_2 and $T_{1\rho}$ was plotted. Percentile values including 80^{th}, 85^{th}, 90^{th} and 95^{th} were explored and we chose to report clusters above the 85^{th} percentile ($12.4mm^2$) as representative of change (Fig. II-C). While the selection of a cluster area threshold is somewhat arbitrary, the 85^{th} percentile appeared to remove noise but still identified focal defects. A metric termed percent cluster area (%CA) was defined as the percent area of the projection map covered by the identified clusters. This was further classified into %CA+ and %CA−; %CA+ is the area covered by clusters with values above the intensity threshold, while %CA− is area covered by clusters with values below the intensity threshold. %CA+ and %CA− were the primary outcome measures of this study (Fig. II-C).

Statistical Analysis

The %CAs calculated from the one-year difference map of the healthy subjects were compared to the %CAs calculated from the six month and one-year difference maps of the ACL-injured subjects. A one-tail, two-sample Wilcoxon signed-rank test was used for comparing the healthy and ACL-injured subjects while a one-tail, one-sample Wilcoxon signed-rank test was used for within ACL-injured subject comparisons. We used a one-tail test because we expect that the %CA's within the ACL-injured population will be greater than those observed within the healthy subjects and we expect that these values will increase over time. This analysis was carried out for both %CA+ and %CA−, of both T_2 and $T_{1\rho}$ relaxation time values. Statistical significance was set at $p < 0.05$ and analysis was performed using packaged software (R package stats, R Foundation for Statistical Computing, Vienna, Austria). Non-parametric analysis was chosen due to the positive skew of the patient data (which violates the assumption of normal distribution) and small sample size.

Short-term (between day 1 and day 2) and long-term (between day 1 and year 1) intra-subject variability as well as intra- (2 repeats) and inter- (2 observers) observer variability measurements were performed on the healthy subject data. Using the difference maps, the pixel-wise and global percent coefficient of variation of the root mean square error ($\%CV_{RMSE}$)[44] were calculated.

To quantify all sources of variability and to properly identify their origin, we analyzed two aspects of intra-session variability: a) consecutive scans without repositioning and b) intrinsic MRI noise. For the first calculation, five additional healthy subjects were scanned twice consecutively and using the same segmentation and projection map technique the $\%CV_{RMSE}$ was determined. For the second calculation, we determined the base level variability introduced to our projection maps due to scanner noise. This consisted of adding repeated measures of appropriately scaled and correlated noise to our acquired data to simulate back-to-back scanning without motion or other variations[45]. First, noise-only data was acquired by switching off the RF excitation in the MRI sequence. These acquired data was used to calculate the covariance matrix that described the Gaussian noise and coupling between the coil elements. We then synthesized Gaussian noise with the same determined statistic and added it to our acquired images. For each synthesis, a projection map was created and the mean $CV_{RMSE}\%$ was calculated for ten back-to-back pairs.

Sensitivity analysis was performed on the healthy subject data to determine the effects of the different sizes of the condyles as well as bone shape changes over time. The radius of each determined best-fit cylinder was varied by ±5% and projection maps were created. The $CV_{RMSE}\%$ was then calculated for each change.

RESULTS

Patient Characteristics and Qualitative Comparisons

Fourteen ACL-injured patients (12 male, 2 female, mean age 32.5 ± 9.8 years, mean height = 1.77 ± 0.1, mean weight = 81.5 ± 9.4, mean BMI = 26.1 ± 2.7 kg/m^2) were included for the final T_2 analysis and seventeen ACL-injured patients (13 male, 4 female, mean age 32.9

± 9.5 years, mean height = 1.75 ± 0.1, mean weight = 82.2 ± 13.4, mean BMI = 26.7 ± 4.3 kg/m^2) for the final $T_{1\rho}$ analysis. Five healthy volunteer (4 male, 1 female, mean age 26.6 ± 2.4 years, mean height = 1.79 ± 0.0, mean weight = 74.5 ± 7.6, mean BMI = 23.3 ± 2.4 kg/m^2) were included for the reproducibility measurements, setting the thresholds and the between group comparisons. One healthy volunteer had to be excluded due to the presence of a cartilage lesion. Motion artifacts excluded three subjects from the ACL-injured T_2 group and incomplete longitudinal data excluded one subject from the $T_{1\rho}$ group.

Intra- and inter-observer reproducibility (CV_{RMSE}%)

All intra- and inter-observer mean global reproducibility measures were less that 9%. The short- and long-term mean intra-subject global CV_{RMSE}% were less than 9% while the intra- and inter-observer mean global CV_{RMSE}% were less than 6% (Table. I). Mean pixel-wise CV_{RMSE}% were less than 15% for the short and long-term intra-subject measures, while the intra- and inter-observer reproducibility were less than 10%.

Intra-session variability

All intra-session variability measures due to consecutive scans and noise were less that 6% for global CV_{RMSE}% and less than 11% for pixel-wise CV_{RMSE}%. The mean pixel-wise CV_{RMSE}% for consecutive scans of five healthy subjects was 8.3 ± 1.7% for T_2 and 6.8 ± 1.1% for $T_{1\rho}$ with their corresponding global CV_{RMSE}% of 4.5 ± 1.8% for T_2 and 3.6 ± 1.7% for $T_{1\rho}$. With added MRI noise and the same segmentation applied to the generated images, the global CV_{RMSE}% was 0.66% and 0.53% and the pixel-wise CV_{RMSE}% was 2.1% and 1.5%, for T_2 and $T_{1\rho}$, respectively. Simulated cylinder radius changes of up to ±5% resulted in global CV_{RMSE}% of less than 1%.

Cluster Analysis

The ACL-injured patients had higher %CA+ for both T_2 and $T_{1\rho}$ relaxation times at six months and one year than the healthy volunteers at one year. Using the healthy volunteer data, thresholds for %CA+ and %CA− were identified as area greater than 12.4mm^2 (Fig. II-C) and value +/−9.0ms and +/−10.8ms for T_2 and $T_{1\rho}$, respectively (Figs. III-B–C and V). For T_2, the six-month ($p=0.0054$) and one year ($p=0.0041$) %CA+ of the ACL-injured group were statistically higher than the one-year %CA+ of the healthy group. For $T_{1\rho}$, a statistical significant difference was observed at one-year between the ACL-injured and the healthy group ($p=0.042$) (Fig. III). In the ACL-injured group, there was an increasing trend from six months to one year, in mean %CA+, for both T_2 (5.2 ± 4.0% to 6.6 ± 3.7%) and $T_{1\rho}$ (6.2 ± 7.1% to 8.2 ± 6.9%), which, for the number of individuals tested, was not statistically significant ($p > 0.05$).

Overall, for the number of individuals tested, no statistically significant differences in %CA − between the injured and healthy groups ($p > 0.1$) and over time within the injured group ($p > 0.1$) were observed. The T_2 %CA− of the ACL-injured group at both six months and one year was comparable to the T_2 %CA− of the healthy group (mean %CA−: 3.0 ± 1.8% & 5.9 ± 5.0% vs. 4.4 ± 4.3%, respectively). ACL-injured patients had higher %CA− at six months and one year for $T_{1\rho}$ than the healthy volunteers (mean %CA−: 4.4 ± 4.9% & 4.5 ± 4.6% vs. 1.9 ± 2.2%, respectively).

DISCUSSION

In this study, we showed differences in T_2 and $T_{1\rho}$ %CAs at six months and one year between the ACL-injured patients and the healthy volunteers. Increasing trends in %CA+ of the ACL-injured group were observed although, over this short time period, they did not reach statistical significance. This novel cluster analysis technique appears to be a useful tool for identifying and tracking focal regions of elevated quantitative MRI values in the ACL-injured population.

The spatial distribution of T_2 and $T_{1\rho}$ relaxation times has been studied using texture and laminar analysis and reports have shown variations in healthy volunteers (up to 5ms from the deep to the superficial layers and between compartments[8,29]) that increase with OA[26,27]. Previous studies have been predominantly limited to one to three slices, usually in the medial and lateral condyles, which are often then subdivided into compartments[23,24]. The voxel-based relaxometry technique[33] has shown the importance of full 3D analysis by assessing $T_{1\rho}$ z-score voxel based patterns of cartilage data that is morphed onto a common template. Our 3D cluster analysis technique on the other hand, identifies focal regions of elevated or decreased quantitative metrics on individual projection maps of averaged pixel data within angular bins. Threshold values of approximately 10ms for both T_2 and $T_{1\rho}$, help in identifying substantial and important focal degenerative lesions rather than describing the heterogeneity. Cluster analysis has been used successfully in functional MRI (fMRI) of the brain to identify activated regions from statistical parametric maps[43]; however, to our knowledge, no previous study has applied this approach to quantitative cartilage data. Combining these two approaches may prove promising.

We calculated six types of variability and found that our global CV_{RMSE}% are comparable to those reported in literature and are lower than changes seen in osteoarthritic cartilage (5ms[11]). For T_2, global CV_{RMSE}% of 5.2% for short-term and 9.0% for long-term are similar to previously reported measurements of between 4–14%[25,47,48]. For $T_{1\rho}$, intra-subject short-term global CV_{RMSE}% of 6.6% and long-term global CV_{RMSE}% of 5.3% fall within reported values of 1.7–8.7% in healthy volunteer studies[24,46,48,49]. The intra-session variability demonstrates that there is some baseline lower bound noise introduced by the scanner and the reported values of 2.1% for T_2 and 1.5% for $T_{1\rho}$ are similar to literature findings for the two sequences of interest[24]. The implication of this finding is that we would expect an underlying contribution of noise to CV% measurements in addition to error due to segmentation, patient motion, registration and other post-processing steps. Overall, our projection map produced similar variability values[24,46–49] as previous studies that looked at the T_2 and $T_{1\rho}$ quantitative measures.

The proposed cluster analysis uses the difference maps from the healthy population to set the intensity threshold and cluster size across populations. The difference maps were key in addressing magic angle effects that could contribute to erroneously identifying regions of elevated T_2 and, to a lesser extent, $T_{1\rho}$ relaxation times. Selecting the 85th percentile cluster size of 12.4mm^2 allowed for characterizing focal lesions by mitigating the effects of noise such as single voxel changes, but still capturing focal lesions. Statistically significant differences were also observed at percentile values of 80, 90 and 95. We were able to

demonstrate changes over time within both T_2 and $T_{1\rho}$ relaxation time maps despite our limited healthy volunteer population size. These thresholding values could be better characterized in the future by tracking particular clusters over time and quantifying the size and intensity changes of these clusters.

Our finding of elevated %CA+ in the ACL population, as compared to our healthy volunteers, is similar to those of previous studies[20–22,37]. Changes did not occur across all patients and were not always consistent when comparing between T_2 and $T_{1\rho}$. With OA changes presenting in approximately 50% of the ACL-injured population[3–6], we would only expect early changes in a subset of our population. Another interesting feature was the presence of decreased cluster areas in T_2 and $T_{1\rho}$ relaxation times over time. Although calculated changes were not statistically significant between groups, the mean %CA− was higher in the ACL-injured group for $T_{1\rho}$. These identified clusters may be worth tracking over a longer period of time.

Our proposed visualization and cluster analysis tool can provide a standardized method of capturing and quantifying changes in quantitative MRI metrics; however, there are some limitations of this study. Motion that could not be corrected using rigid body registration, excluded data from further analysis. Segmentation was performed twice to account for any motion in between scans, however this added to the manual processing time. In addition, registration utilized interpolation, which may introduce some blurring; however, we expect that the threshold choices in our analysis help mitigate introduced errors. Although the cylinder was fit to the cartilage-bone boundary, the condyles of the lateral and medial side are not the same size and some studies have shown that there are changes in bone shape as early as three months after injury with statistical significant changes observed over five years in the ACL-injured population[50]. However, simulations carried out to understand the potential effect of the difference in condyle size and bony changes found that CV_{RMSE}% in the projection maps was less than 1%. Over longer periods of time, bone shape changes should be monitored. Some areas of cartilage were not segmented due to metal-induced artifacts and this lead to incomplete cartilage plates (< 15% removed) with possible clusters being missed. However, this was not of great concern, as complete cartilage would only increase the differences observed. Finally, no pre-surgery baseline data was collected for this study, however it is unclear what the effect of post-surgery edema will have on quantitative cartilage values.

In conclusion, we have demonstrated that our cluster analysis technique can identify focal changes in the ACL-injured population over time. Our results show promise for detecting and tracking early degenerative changes in a robust, objective manner. This tool may further help with understanding the cartilage degeneration process and serve in monitoring the effectiveness of therapeutic approaches for OA.

Supplementary Material

Refer to Web version on PubMed Central for supplementary material.

Acknowledgments

The authors gratefully acknowledge Weitian Chen for technical assistance during the CubeQuant T1rho acquisitions, Bragi Sveinsson for his assistance with the qDESS computations, Dr. Jarrett Rosenbery for his help with the statistical design and analysis and Dr. Jason Dragoo and Hillary Braun for help with recruiting the ACL-injured patients.

Role of the funding source

This project was supported by the following: the National Institutes of Health (Grant Numbers R01-EB002524, K24-AR062068, and R01-AR0063643, P41-EB015891), the Arthritis Foundation, the Stanford Diversifying Academia, Recruiting Excellence Graduate Research Fellowship and GE Healthcare. The study sponsors had no involvement in the study design, collection, analysis, or interpretation of data, nor in the decision to submit the manuscript for publication.

References

1. Centers for Disease Control & Prevention, National Center for Health Statistics. National hospital discharge survey: annual summary 1996 [monograph on the Internet]. Atlanta, GA: Centers for Disease Control and Prevention; 1996.
2. Øiestad BE, Engebretsen L, Storheim K, Risberg MA. Knee osteoarthritis after anterior cruciate ligament injury: a systematic review. Am J Sports Med. 2009; 37(7):1434–43. [PubMed: 19567666]
3. Lohmander LS, Ostenberg A, Englund M, Roos H. High prevalence of knee osteoarthritis, pain, and functional limitations in female soccer players twelve years after anterior cruciate ligament injury. Arthritis Rheum. 2004; 50(10):3145–3152. [PubMed: 15476248]
4. von Porat A, Roos EM, Roos H. High prevalence of osteoarthritis 14 years after an anterior cruciate ligament tear in male soccer players: a study of radiographic and patient relevant outcomes. Ann Rheum Dis. 2004; 63(3):269–273. [PubMed: 14962961]
5. van der Hart C, van den Bekerom M, Patt T. The occurrence of osteoarthritis at a minimum of ten years after reconstruction of the anterior cruciate ligament. J Orthop Surg Res. 2008; 3:24. [PubMed: 18544170]
6. Lohmander LS, Englund PM, Dahl LL, Roos EM. The long-term consequence of anterior cruciate ligament and meniscus injuries: osteoarthritis. Am J Sports Med. 2007; 35(10):1756–1769. [PubMed: 17761605]
7. Regatte RR, Akella SV, Borthakur A, Kneeland JB, Reddy R. Proteoglycan depletion-induced changes in transverse relaxation maps of cartilage: comparison of T2 and T1rho. Acad Radiol. 2002; 9:1388e94. [PubMed: 12553350]
8. Dardzinski BJ, Mosher TJ, Li S, Van Slyke MA, Smith MB. Spatial variation of T2 in human articular cartilage. Radiology. 1997; 205:546e50. [PubMed: 9356643]
9. Regatte RR, Akella SV, Lonner JH, Kneeland JB, Reddy R. T1rho relaxation mapping in human osteoarthritis (OA) cartilage: comparison of T1rho with T2. J Magn Reson Imaging. 2006; 23:547e53. [PubMed: 16523468]
10. Stahl R, Blumenkrantz G, Carballido-Gamio J, Zhao S, Munoz T, Hellio Le Graverand-Gastineau MP, et al. MRI-derived T2 relaxation times and cartilage morphometry of the tibio-femoral joint in subjects with and without osteoarthritis during a 1-year follow-up. Osteoarthritis Cartilage. 2007; 15:1225e34. [PubMed: 17561417]
11. Li X, Benjamin Ma C, Link TM, Castillo DD, Blumenkrantz G, Lozano J, et al. In vivo T(1rho) and T(2) mapping of articular cartilage in osteoarthritis of the knee using 3 T MRI. Osteoarthritis Cartilage. 2007; 15:789e97. [PubMed: 17307365]
12. Duvvuri U, Kudchodkar S, Reddy R, et al. T(1rho) relaxation can assess longitudinal proteoglycan loss from articular cartilage in vitro. Osteoarthritis Cartilage. 2002; 10:838–44. [PubMed: 12435327]
13. Regatte RR, Akella SV, Borthakur A, et al. Proton spin-lock ratio imaging for quantitation of glycosaminoglycans in articular cartilage. J Magn Reson Imaging. 2003; 17:114–21. [PubMed: 12500280]

14. Nishioka J, Hirose J, Nakamura E, et al. T1ρ and T2 mapping reveal the in vivo extracellular matrix of articular cartilage. J Magn Reson Imaging. 2012; 35:147–55. [PubMed: 21990043]
15. Wong CS, Yan CH, Gong NJ, Li T, Chan Q, Chu YC. Imaging biomarker with T1ρ and T2 mappings in osteoarthritis - in vivo human articular cartilage study. Eur J Radiol. 2013; 82(4):647–50. [PubMed: 23333531]
16. Tsushima H, Okazaki K, Takayama Y, Hatakenaka M, Honda H, Izaawa T, et al. Evaluation of cartilage degradation in arthritis using T1ρ magnetic resonance imaging mapping. Rheumatol Int. 2012; 32(9):2867–75. [PubMed: 21881979]
17. Duvvuri U, Reddy R, Patel SD, Kaufman JH, Kneeland JB, Leigh JS. T1rho-relaxation in articular cartilage: effects of enzymatic degradation. Magn Reson Med. 1997; 38(6):863–867. [PubMed: 9402184]
18. Mosher TJ, Dardzinski BJ, Smith MB. Human articular cartilage: influence of aging and early symptomatic degeneration on the spatial variation of T2—preliminary findings at 3 T. Radiology. 2000; 214(1):259–66. [PubMed: 10644134]
19. Dunn TC, Lu Y, Jin H, Ries MD, Majumdar S. T2 relaxation time of cartilage at MR imaging: comparison with severity of knee osteoarthritis. Radiology. 2004; 232(2):592–8. [PubMed: 15215540]
20. Bolbos RI, Ma CB, Link TM, Majumdar S, Li X. In vivo T1rho quantitative assessment of knee cartilage after anterior cruciate ligament injury using 3 Tesla magnetic resonance imaging. Invest Radiol. 2008; 43(11):782–8. [PubMed: 18923257]
21. Li X, Kuo D, Theologis A, Carballido-Gamio J, Stehling C, Link TM, et al. Cartilage in anterior cruciate ligament-reconstructed knees: MR imaging T1{rho} and T2–initial experience with 1-year follow-up. Radiology. 2011; 258(2):505–514. [PubMed: 21177392]
22. Su F, Hilton JF, Nardo L, Wu S, Liang F, Link TM, et al. Cartilage Morphology and T1rho and T2 Quantification in ACL-reconstructed Knees: A 2-year Follow-up. Osteoarthritis Cartilage. 2013; 21(8):1058–1067. [PubMed: 23707754]
23. Klocke NF, Amendola A, Thedens DR, Williams GN, Luty CM, Martin JA, et al. Comparison of T1ρ, dGEMRIC, and quantitative T2 MRI in preoperative ACL rupture patients. Acad Radiol. 2013; 20(1):99–107. [PubMed: 22981604]
24. Jordan CD, McWalter EJ, Monu UD, Watkins RD, Chen W, Bangerter NK, et al. Variability of CubeQuant T1ρ, quantitative DESS T2, and cones sodium MRI in knee cartilage. Osteoarthritis Cartilage. 2014; 22:1559–1567. [PubMed: 25278065]
25. Goodwin DW, Wadghiri YZ, Dunn JF. Micro-imaging of articular cartilage: T2, proton density, and the magic angle effect. Acad Radiol. 1998; 5:790–798. [PubMed: 9809078]
26. Blumenkrantz, G., Dunn, TC., Carballido-Gamio, J., Link, TM., Majumdar, S. Spatial Heterogeneity of Cartilage T2 in Osteo-arthritic Patients. Boston, MA: OARSI; 2005.
27. Carballido-Gamio J, Stahl R, Gabrielle B, Adan R, Sharmila M. Spatial analysis of magnetic resonance T1rho and T2 relaxation times improves classification between subjects with and without osteoarthritis. Med Phys. 2009; 36:4059–67. [PubMed: 19810478]
28. Joseph GB, Baum T, Alizai H, Carballido-Gamio J, Nardo L, Virayavanich W, et al. Texture analysis of cartilage T2 maps: individuals with risk factors for OA have higher and more heterogeneous knee cartilage MR T2 compared to normal controls –data from the osteoarthritis initiative. Arthritis Res Ther. 2011; 13(5):R153. Epub 2011 Sep 20. doi: 10.1186/ar3469 [PubMed: 21933394]
29. Smith HE, Mosher TJ, Dardzinski BJ, Collins BG, Collins CM, Yang QX, et al. Spatial variation in cartilage T2 of the knee. J Magn Reson Imaging. 2001; 14:50–55. [PubMed: 11436214]
30. Carballido-Gamio J, Link TM, Majumdar S. New techniques for cartilage magnetic resonance imaging relaxation time analysis: texture analysis of flattened cartilage and localized intra- and inter-subject comparisons. Magn Reson Med. 2008; 59:1472–1477. [PubMed: 18506807]
31. Li X, Pai A, Blumenktrantz G, Carballido-Gamio J, Link T, Ma B, et al. Spatial distribution and relationship of T1rho and T2 relaxation times in knee cartilage with osteoarthritis. Magn Reson Med. 2009; 61(6):1310–8. [PubMed: 19319904]

32. Blumenkrantz G, Stahl R, Carballido-Gamio J, Zhao S, Munoz T, Hellio Le Graverand-Gastineau M-P, et al. The feasibility of characterizing the spatial distribution of cartilage T2 using texture analysis. Osteoarthritis Cartilage. 2008; 16(5):584–590. [PubMed: 18337129]
33. Pedoia V, Li X, Su F, Calixto N, Majumdar S. Fully automatic analysis of the knee articular cartilage T1<rho> relaxation time using voxel-based relaxometry. J Magn Reson Imaging. 2016; 43:970–980. [PubMed: 26443990]
34. Akhtar S, Poh CL, Kitney RI. An MRI derived articular cartilage visualization framework. Ostoearthritis Cartilage. 2007; 15:1070–85.
35. Duryea J, Iranpour-Boroujeni T, Collins JE, Vanwynngaarden C, Guermazi A, Katz JN, et al. Local-Area Cartilage Segmentation (LACS), A Semi-Automated Novel Method of Measuring Cartilage Loss in Knee Osteoarthritis. Arthritis Care Res. 2014; 66(10):1560–1565.
36. Mosher TJ, Dardzinski BJ, Smith MB. Human articular cartilage: influence of aging and early symptomatic degeneration on the spatial variation of T2—preliminary findings at 3 T. Radiology. 2000; 214:259–266. [PubMed: 10644134]
37. Jordan, CD. PhD Thesis. Stanford University; 2013. Evaluation and Application of Novel Tools for Muskuloskeletal and Body MRI.
38. Chen W, Takahashi A, Han ET. 3D quantitative imaging of T1rho and T2 (Abstract). Proc Annual Meeting ISMRM. 2011; 231
39. Rosset. OsiriX: An Open-Source Software for Navigating in Multidimensional DICOM Images. J Digit Imaging. 2004 Sep; 17(3):205–216. [PubMed: 15534753]
40. Staroswiecki E, Granlund KL, Alley MT, Gold GE, Hargreaves BA. Simultaneous estimation of T(2) and apparent diffusion coefficient in human articular cartilage in vivo with a modified three-dimensional double echo steady state (DESS) sequence at 3 T. Magn Reson Med. 2012; 67:1086e96. [PubMed: 22179942]
41. Matzat SJ, McWalter EJ, Kogan F, Chen W, Gold GE. T2 Relaxation time quantitation differs between pulse sequences in articular cartilage. J Magn Reson Imaging. 2015; 42:105–113. [PubMed: 25244647]
42. Welsch GH, Mamisch TC, Zak L, et al. Morphological and biochemical T2 evaluation of cartilage repair tissue based on a hybrid double echo at steady state (DESS-T2d) approach. J Magn Reson Imaging. 2011; 34:895–903. [PubMed: 21769974]
43. Mezer A, Yovel Y, Pasternak O, Gorfine T, Assaf Y. Cluster analysis of resting-state fMRI time series. NeuroImage. 2009:1117–1125. [PubMed: 19146962]
44. Glüer CC, Blake G, Lu Y, Blunt BA, Jergas M, Genant HK. Accurate assessment of precision errors: how to measure the reproducibility of bone densitometry techniques. Osteoporos Int. 1995; 5:262e70. [PubMed: 7492865]
45. Peter K, Elliot RM. Image Reconstruction in SNR Units: A General Method for SNR Measurement. Magn Reson Med. 2005; 54(6):1439–1447. [PubMed: 16261576]
46. Li X, Han ET, Busse RF, Majumdar S. In vivo T(1rho) mapping in cartilage using 3D magnetization-prepared angle-modulated partitioned k-space spoiled gradient echo snapshots (3D MAPSS). Magn Reson Med. 2008; 59:298e307. [PubMed: 18228578]
47. Mosher TJ, Zhang Z, Reddy R, Boudhar S, Milestone BN, Morrison WB, et al. Knee articular cartilage damage in osteoarthritis: analysis of MR image biomarker reproducibility in ACRIN-PA 4001 multicenter trial. Radiology. 2011; 258(3):832e42. [PubMed: 21212364]
48. Li X, Wyatt C, Rivoire J, Han ET, Chen W, Schooler J, et al. Simultaneous acquisition of T1ρ and T2 quantification in knee cartilage: repeatability and diurnal variation. J Magn Reson Imaging. 2014; 39(5):1287e93. [PubMed: 23897756]
49. Li X, Han ET, Busse RF, Majumdar S. In vivo T(1rho) mapping in cartilage using 3D magnetization-prepared angle-modulated partitioned k-space spoiled gradient echo snapshots (3D MAPSS). Magn Reson Med. 2008; 59:298e307. [PubMed: 18228578]
50. Hunter DJ, Lohmander LS, Makovey J, Tamez-Pena J, Totterman S, Schreyer E, Frobell RB. The Effect of Anterior Cruciate Ligament Injury on Bone Curvature: Exploratory Analysis in the KANON Trial. Osteoarthritis Cartilage. 2014; 22(7):959–968. [PubMed: 24867633]

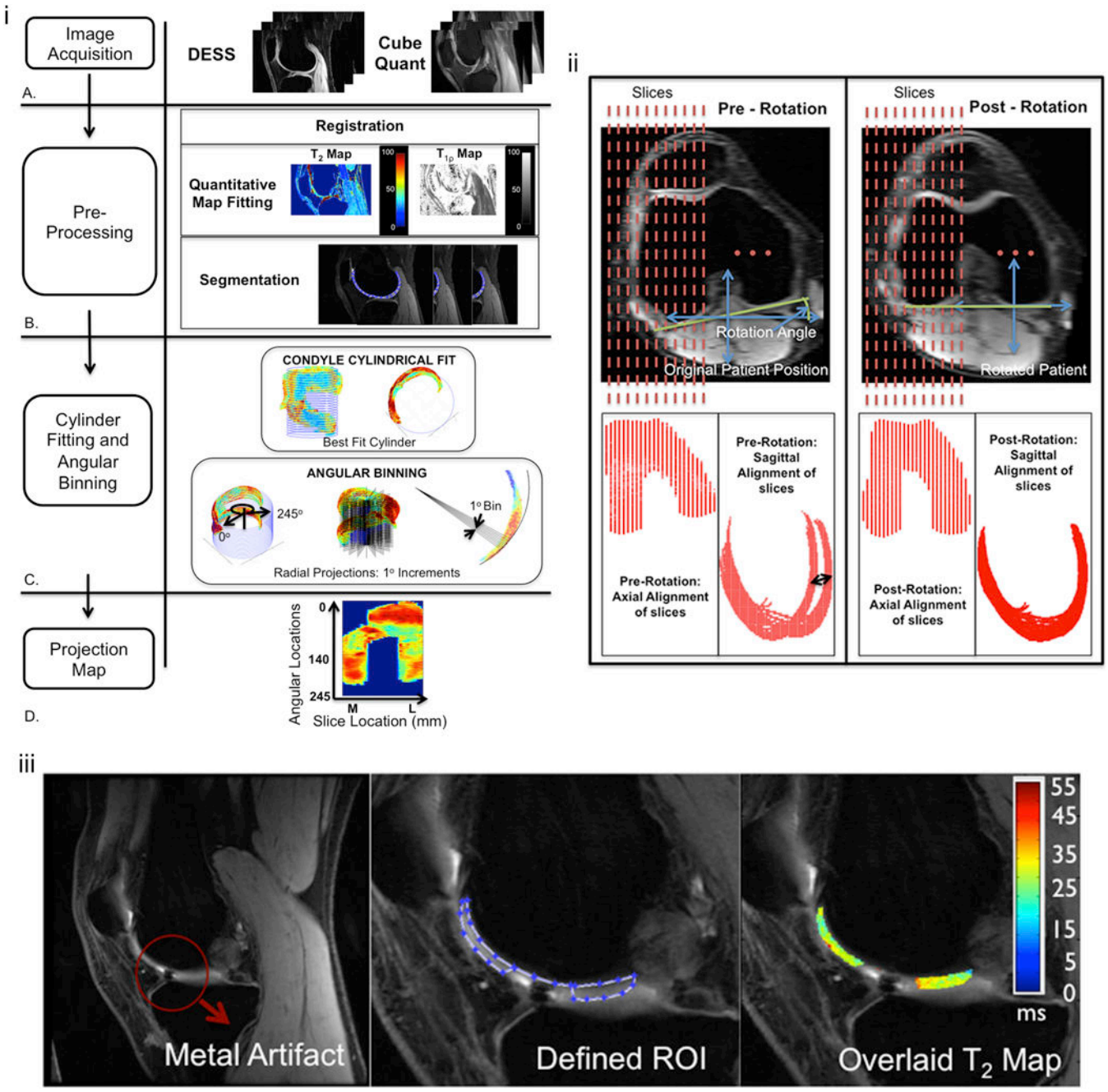

Figure I.

i. The methods flow chart shows the image acquisition using the DESS and Cubequant sequences (A), the pre-processing steps involving registration, quantitative map fitting and 3D manual segmentation (B) and the best fit cylinder and unwrapping of the cartilage using radial projection lines (C) to create a projection map plotting the angular location of the cartilage against the slice width in mm (D).

ii. Registration: Axial rotation and re-slicing of the knee to define the anatomically based sagittal plane perpendicular to the tangential line through the most posterior points of the femoral condyles and slices of equal longitudinal coverage across the knee. Pre-rotation

sagittal images demonstrate the misalignment of the posterior condyles (black arrow) that is corrected after rotation.

iii. Manual Segmentation: Sample ACL-injured patient with a metal artifact in one of the slices. During segmentation, sufficient distance to the artifact was left so that no signal pileup or void was captured.

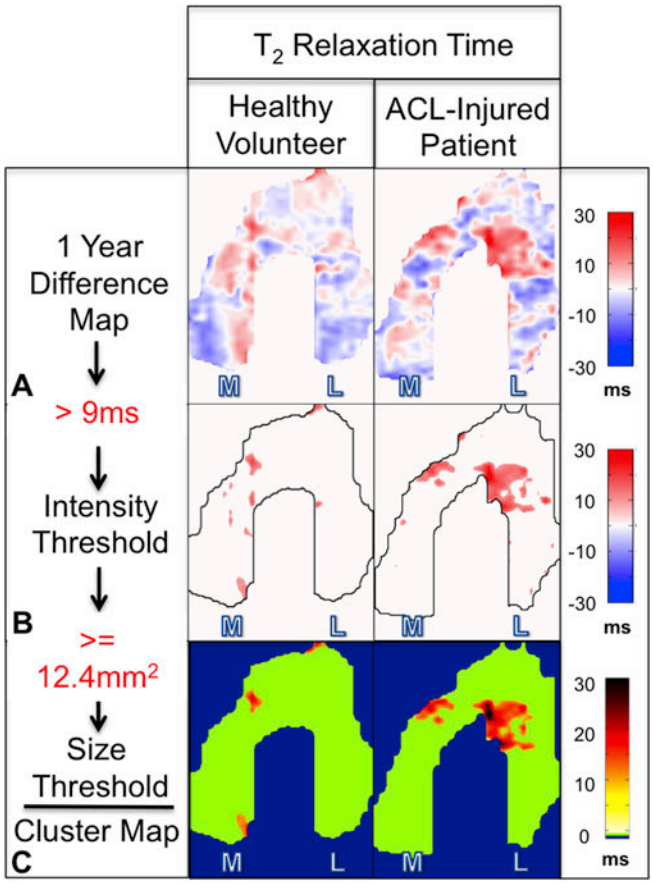

Figure II.

Cluster map pipeline showing the difference maps (A) used with the determined intensity (B) and area (C) thresholds to create the final cluster map.

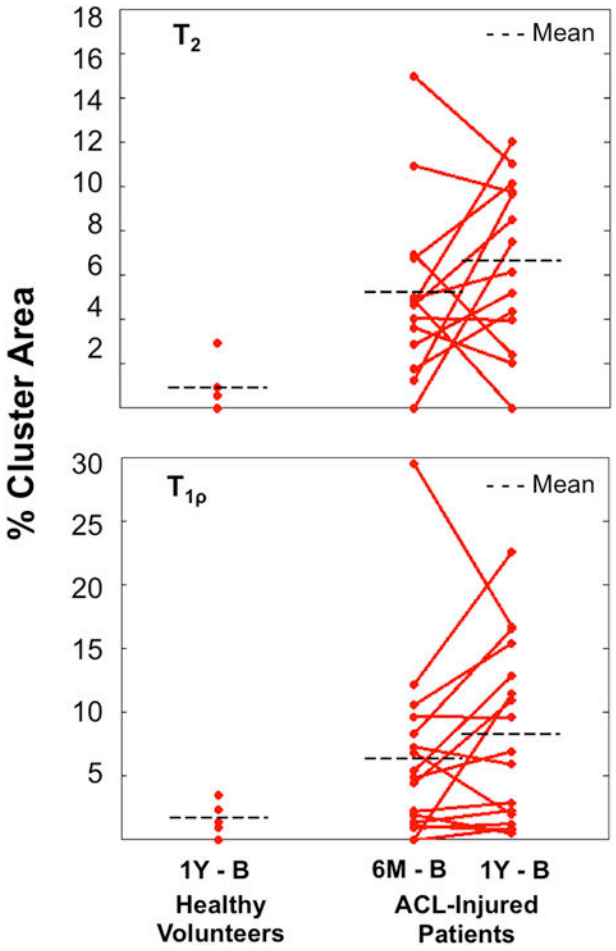

Figure III.

% Cluster Areas of projection maps covered by clusters in the ACL-injured population for both T_2 and $T_{1\rho}$ as compared to the healthy volunteers. A T_2 elevation threshold of +9ms and a $T_{1\rho}$ elevation threshold of +10.8ms was applied at 6 months and 1 year with individual %CA's shown in 14 (T_2) and 17 ($T_{1\rho}$) ACL-injured patients and averaged %CA's shown in both populations.

Table I

Intra-subject (short and long term), intra-observer (short term) and inter-observer (short term) RMSE Coefficient of Variation (%) of T_2 and $T_{1\rho}$ measurements.

Volunteer	Intra-subject Short-term	Intra-subject Long-term	Intra-observer Short-term	Inter-observer Short-term
T_2 Measurements (%CV_{RMSE})				
GLOBAL MEAN	5.2 (± 0.9)	9.0 (± 2.8)	3.5 (± 1.5)	5.3 (± 1.2)
GLOBAL RANGE	[4.1–6.3]	[6.6–13.7]	[2.0–5.2]	[4.1–6.6]
PIXEL-WISE MEAN	10.8 (± 1.0)	14.6 (± 3.0)	5.8 (± 1.8)	9.3 (± 2.9)
PIXEL-WISE RANGE	[9.2–11.8]	[11.8–19.6]	[4.0–8.3]	[6.5–11.1]
$T_{1\rho}$ Measurements (%CV_{RMSE})				
GLOBAL MEAN	6.6 (± 3.2)	5.3 (± 1.1)	2.3 (± 0.5)	3.6 (± 0.5)
GLOBAL RANGE	[3.6–10.4]	[4.3–6.9]	[1.6–2.8]	[2.8–4.1]
PIXEL-WISE MEAN	12.2 (± 2.7)	12.3 (± 2.4)	5.0 (± 1.6)	7.1 (± 0.9)
PIXEL-WISE RANGE	[9.2–15.0]	[9.5–15.3]	[3.1–7.5]	[5.6–7.9]